Research Square

Preprints are preliminary reports that have not undergone peer review.
They should not be considered conclusive, used to inform clinical practice,
or referenced by the media as validated information.

Enhancing Prediction of Pathological Complete Response to Neoadjuvant Immunotherapy in Non-small cell lung cancer by Whole Lung Radiomics

Xiaoting Cai
Tianjin Medical University Cancer Institute and Hospital
Jingyi Yang
Tianjin Medical University Cancer Institute and Hospital
Fangyuan Qu
Tianjin Medical University Cancer Institute and Hospital
Qiliang Wang
Tianjin Medical University Cancer Institute and Hospital
Jiahui E
Tianjin Medical University Cancer Institute and Hospital
Fan Liu
Tianjin Medical University Cancer Institute and Hospital
Yicai Zhang
Tianjin Medical University Cancer Institute and Hospital
Bingsheng Sun
Tianjin Medical University Cancer Institute and Hospital
Ying Liu
tjliuying2009@163.com

Tianjin Medical University Cancer Institute and Hospital

Research Article

Keywords: Non-small cell lung cancer, Neoadjuvant immunotherapy, Radiomics, Pathological complete response

Posted Date: April 9th, 2026

DOI: https://doi.org/10.21203/rs.3.rs-9078017/v1

License: This work is licensed under a Creative Commons Attribution 4.0 International License.
Read Full License

Additional Declarations: No competing interests reported.

Version of Record: A version of this preprint was published at BMC Cancer on September 10th, 2026. See the published version at https://doi.org/10.1186/s12885-026-16939-7.

Abstract

Objective

To evaluate the utility of whole lung radiomics for predicting pathological complete response (pCR) to neoadjuvant immunotherapy in patients with non-small cell lung cancer (NSCLC). We further investigated whether integrating whole lung radiomics with tumor-specific radiomics could enhance the predictive performance for pCR.

Methods

Consecutive patients with stage II-IIIB NSCLC who underwent neoadjuvant immunotherapy were retrospectively enrolled between August 2018 and June 2025. The intra-tumoral and whole lung radiomics features were extracted from baseline CT images. Radiomics models were constructed using the LightGBM classifier. Model performance was assessed using receiver operating characteristic (ROC) curve, and recurrence-free survival (RFS) outcomes were evaluated via Kaplan-Meier survival analysis.

Results

A total of 284 patients (median age [IQR], 62 [57–67] years; 239 men) were enrolled and subsequently randomized into a training cohort (n = 199) and a test cohort (n = 85). Among them, 124 patients (43.7%) achieved pCR after neoadjuvant immunotherapy. The combined model, which incorporates 6 tumor-specific radiomics features, 3 whole lung derived radiomics features, and a clinical indicator (carcinoma embryonic antigen, CEA), achieved areas under the curve (AUC) of 0.713 (95% CI: 0.600–0.827), sensitivity of 83.3%, and specificity of 63.6% in the test cohort. Patients classified as low-risk group by the combined model exhibited significantly prolonged RFS (log-rank $P < 0.05$).

Conclusion

The proposed whole lung radiomics approach demonstrates potential for predicting pCR to neoadjuvant immunotherapy in NSCLC. The combined model has capability to predict therapeutic response and prognosis prior to the initiation of neoadjuvant immunotherapy, enabling non-invasive personalized prediction.

Introduction

In recent years, immune checkpoint inhibitors (ICIs) have reshaped the treatment landscape for non-small cell lung cancer (NSCLC). The integration of ICIs with conventional chemotherapy in neoadjuvant chemoimmunotherapy regimens has yielded compelling clinical outcomes, as evidenced by substantial tumor downstaging, increased R0 resection rates, and a notable reduction in disease recurrence risks [1].

Pathological complete response (pCR), defined as the absence of viable tumor cells in both the resected primary tumor and sampled regional lymph nodes, has been validated as a reliable surrogate endpoint for predicting survival benefits [2]. Several randomized controlled trials have reported encouraging pCR rates, ranging from 24.8% to 37% for patients with NSCLC receiving neoadjuvant chemoimmunotherapy [3, 4]. While these efficacy outcomes are promising, comprehensive treatment evaluation must also consider safety profiles. Notably, the administration of ICIs carries a potential risk of inducing immune-related adverse events (irAEs) [5]. Therefore, there is an urgent imperative to develop individualized predictive biomarkers capable of identifying patients who are likely to benefit from neoadjuvant chemoimmunotherapy before treatment initiation.

Radiomics represents an advanced computational methodology that enables the non-invasive and comprehensive analysis of high-dimensional medical imaging data, facilitating the extraction of a substantial array of quantitative sub-visual features that lie beyond the discernment capabilities of human vision. This innovative technique has been widely employed in the prediction and evaluation of therapeutic efficacy for various tumor types, thereby demonstrating its extensive clinical utility [6–9]. Previous studies have confirmed that pretreatment radiomics features derived from tumor regions can serve as potential biomarkers for predicting response to neoadjuvant chemoimmunotherapy in NSCLC [10, 11]. These findings accentuate the escalating clinical relevance of radiomics in the field of oncology, presenting a promising pathway for enhancing treatment decision-making through imaging-based evaluations.

Chronic respiratory diseases, especially chronic obstructive pulmonary disease (COPD), have been confirmed as a risk factor for the development of lung cancer. The coexistence of these two conditions, known as lung cancer combined with COPD (LC-COPD), represents a clinically relevant and frequently encountered comorbidity [12]. Emerging evidence suggests that patients with LC-COPD may derive greater therapeutic benefits from immunotherapy, with improved survival outcomes compared to those without underlying COPD [13–16]. The assessment of COPD through conventional CT imaging remains challenging due to its poor consistency and subjective interpretation, which often leads to unreliable diagnostic outcomes. A recent study demonstrated that CT-based whole lung radiomics analysis exhibited optimal performance in identifying COPD [17], highlighting its potential as an objective and quantitative tool. A multicenter study further demonstrated that whole lung radiomics features were associated with overall survival in patients with locally advanced NSCLC treated with definitive chemoradiotherapy [18], supporting their role in therapeutic efficacy evaluation in lung cancer. At present, the utility of CT-based whole lung radiomics for predicting treatment response to neoadjuvant immunotherapy in NSCLC remains unexplored.

We hypothesize that the quantitative extraction of imaging biomarkers from the entire lung parenchyma may provide clinically relevant diagnostic insights, facilitating the detection of subtle radiological patterns that may be associated with therapeutic outcomes. The aim of this study was to explore the predictive utility of baseline whole lung radiomics in predicting treatment response to neoadjuvant immunotherapy for NSCLC. Furthermore, we integrated whole lung radiomics with tumoral radiomics to

develop a comprehensive predictive model to guide personalized therapeutic strategies for NSCLC patients.

Materials and methods

Study cohort

This retrospective study was approved by the Institutional Review Board (Approval No. bc20260290), and the requirement for written informed consent was waived. All data were processed in strict compliance with HIPAA regulations. We anonymized the datasets by removing direct identifiers (names, IDs) and performed data minimization, retaining only the variables necessary for the analysis. According to the inclusion and exclusion criteria, a total of 284 patients with stage II-IIIB NSCLC patients who underwent curative surgery after neoadjuvant immunotherapy were enrolled between August 2018 and June 2025 (Fig. 1, Supplementary Text 1). The patients were randomly allocated to the training cohort and the test cohort in a 7:3 ratio. The whole study flow chart is shown in Fig. 2.

Clinical and pathological data were retrieved from the electronic medical record system, including gender, age, smoking history, tumor size, histologic type, TNM stage, treatment regimen, treatment cycle, lymph node status, and tumor burden. Laboratory data, including complete blood count and lung tumor markers, obtained within two weeks prior to the initiation of neoadjuvant immunotherapy treatment, were collected (Supplementary Text 2). The TNM stage was assessed according to the 9th edition of the American Joint Committee on Cancer staging system [19].

All patients received neoadjuvant therapy that primarily consisted of ICIs (nivolumab, pembrolizumab, or Atezolizumab), administered either as monotherapy or in combination with platinum-based chemotherapy (cisplatin or carboplatin combined with paclitaxel or pemetrexed). The regimen was delivered at 3-week intervals for a total of 2 to 5 cycles prior to surgical intervention. Surgical resection was performed within 4 weeks following the completion of neoadjuvant immunotherapy.

Pathological assessments and follow-up

Pathological complete response (pCR) was defined as the absence of residual viable tumor in the tumor bed (including primary tumor bed and sampled lymph nodes, ypT0 and ypN0). Based on postoperative pathological findings, patients were stratified into either pCR or non-pCR group. Postoperative routine follow-ups were performed at intervals of every 3 to 6 months during the first two years following surgery, and every 6 to 12 months thereafter until death or the last follow-up date (January 15, 2026). Chest CT examinations were performed during clinical visits or when disease recurrence was suspected. For patients presenting with specific clinical symptoms, targeted imaging of the affected anatomical sites was performed using the most appropriate imaging modalities. Recurrence-free survival (RFS) was defined as the time from surgery to tumor recurrence or death from any cause [20, 21].

CT image acquisition

All participants underwent CT examinations with the following equipment: GE Medical Systems (Discovery CT750 HD, Optima 680 Expert, and Revolution EVO), Siemens (SOMATOM Definition AS + and SOMATOM Drive), and Philips (IQon spectral CT). The imaging acquisition parameters were configured as follows: reconstruction thicknesses of 1.25 mm or 1.5 mm, tube voltage of 120 kV, tube current of 150 to 200 mAs, and a matrix size of 512 × 512. Image acquisition was performed at the end-inspiratory phase to minimize respiratory motion artifacts.

Image analysis

Tumor burden is quantified by calculating the sum of diameters for selected target lesions under Response Evaluation Criteria in Solid Tumors (RECIST) guidelines [22]. The detailed methodology is as follows: Target lesions are defined as measurable tumor lesions with the longest diameter ≥ 10 mm (on CT scans with a slice thickness ≤ 5 mm) and lymph nodes with the maximum short-axis diameter ≥ 15 mm. The number of target lesions is restricted to a maximum of 2 per organ and 5 in total across all organs. Priority is given to selecting the largest, reproducibly measurable lesions covering all involved organs.

Methods for assessing lymph node status are as follows: Traditional enlarged lymph nodes were defined as measurable lymph nodes with the maximum short-axis diameter ≥ 10 mm, whereas RECIST-defined enlarged lymph nodes were defined as measurable lymph nodes with the maximum short-axis diameter ≥ 15 mm [22].

ROI segmentation

To mitigate the influence of slice thickness on radiomics feature stability, all CT images were isotropically resampled to a uniform 1 mm^3 voxel dimension using linear interpolation. The 3D slicer software (v5.6.1; https://download.slicer.org) was used to manually delineate tumor regions of interest (ROIs) slice-by-slice on axial CT images. Intra- and inter-observer variabilities were assessed using 30 randomly selected CT datasets. The segmentations were performed by an initial observer (X.T.C., with 5 years of experience) and repeated after 4 weeks for intra-observer analysis. For inter-observer analysis, a second radiologist (J.Y.Y., with 3 years of experience) independently performed segmentation on the same 30 cases. To ensure feature robustness, only those with an intraclass correlation coefficient (ICC) ≥ 0.75 were retained for subsequent analyses. Bilateral lung ROIs were initially segmented utilizing a publicly available deep learning model (https://github.com/JoHof/lungmask), followed by manual refinement by an experienced radiologist. The final whole lung ROI for radiomics analysis was obtained by subtracting the primary tumor ROI from these refined bilateral lung ROIs.

Radiomic features extraction and feature selection

Radiomics features were extracted from both tumor and whole lung regions using FeAture Explorer (FAE, version 0.5.16), an open-source software based on the PyRadiomics framework (Fig. S1). All radiomics features were normalized using Z-score standardization. A four-step feature selection pipeline was implemented to identify non-redundant radiomics features. Initially, preliminary feature screening was conducted using either the Student's t-test or the Mann-Whitney U test, depending on data distribution. Features showing statistical significance ($P < 0.05$) were subsequently evaluated using Pearson correlation analysis. For highly correlated feature pairs (correlation coefficient > 0.9), only one feature was retained to mitigate multicollinearity. The Minimum Redundancy Maximum Relevance (MRMR) algorithm was then applied to further refine the feature set by maximizing discriminatory power while minimizing redundancy. Finally, the Least Absolute Shrinkage and Selection Operator (LASSO) method was employed to identify the most predictive feature subset through rigorous feature selection.

Development of prediction models

Three radiomics models, including the primary tumor radiomics model (PT), the whole lung radiomics model (WL), and the primary tumor plus whole lung radiomics model (PTWL), were constructed using the LightGBM classifier with 10-fold cross-validation. The discriminative performance of the model was evaluated using the receiver operating characteristic (ROC) curve, and the model exhibiting the highest area under the curve (AUC) value on the test cohort was identified as the optimal model.

Statistical analysis

The statistical analyses were conducted using R software (v4.4.1, http://www.R-project.org) and SPSS software (v27.0, IBM SPSS Statistics). To determine the minimal sample size required for the analysis, the null hypothesis was set at an AUC of 0.50, and the alternate hypothesis at an AUC of 0.70, with a desired statistical power of 90% [23]. Based on the group proportions of 37% for pCR and 63% for non-pCR, the resulting minimal sample size was 90 participants, comprising 33 pCR cases and 57 non-pCR cases. Categorical variables were compared using Pearson's $\chi 2$ test or Fisher's exact test, whereas continuous variables were analyzed using Student's t-test or Mann–Whitney U test, depending on their distribution characteristics. Variables with $P < 0.05$ in univariable analysis were included in the multivariable logistic regression. Comparisons of AUC values were conducted using the DeLong test. The calibration of the model was assessed with the Hosmer–Lemeshow test. Decision curve analysis (DCA) was performed to assess the clinical utility of the model. To determine the incremental predictive value, the integrated discrimination improvement (IDI) and net reclassification index (NRI) were calculated at cutoffs of 0, 0.4, and 1, using the PredictABEL package (v1.2). Kaplan-Meier survival analysis and log-rank tests were applied to evaluate differential survival outcomes between patients achieving pCR and those with non-pCR. A two-sided P-value < 0.05 was considered statistically significant.

Results

Clinicopathological characteristics

Table 1 and 2 summarize the baseline characteristics of the 284 patients (median age [interquartile range, IQR], 62 [57–67] years) enrolled in this study. There were no statistically significant differences ($P > 0.05$) in terms of clinicopathological features between the training cohort (n = 199) and the test cohort (n = 85), which supports the comparability of the two cohorts for subsequent analyses. All patients underwent curative surgical resection and pCR was achieved in 124 patients (43.7%) according to postoperative histopathological results. Univariable analysis showed that histologic type and tumor biomarkers—including CEA and Cyfra21-1—were significantly associated with pCR (all $P < 0.05$). Multivariable analysis revealed that CEA was the independent risk factor for pCR (odds ratio [OR] 0.447; 95% confidence interval [CI]: 0.209 - 0.956], $P < 0.05$) (Table S1). Moreover, the predictive performance of the clinical model based on CEA for predicting pCR yielded an AUC of 0.597 in the training cohort and 0.559 in the test cohort, respectively (Fig. 3A-3B).

Radiomics feature selection

After eliminating 243 tumor radiomics features exhibiting poor repeatability (ICC < 0.75), feature dimensionality reduction and selection procedures were performed. The tumor and whole lung radiomics signatures were composed of 5 and 3 radiomics features, respectively. The integrated radiomics signature, derived from the fusion of tumor-specific and whole lung radiomics features, retained a total of 9 radiomics features, including 6 features extracted from the tumor region and 3 features derived from the whole lung region. The detailed information is presented in Supplementary Text 3 and Table S2-S4.

Predictive performance of the models

The performance metrics of all radiomics models are presented in Table 3. The PTWL model, which incorporated primary tumor and whole lung radiomics features, showed superior performance with AUCs of 0.792 (95% CI: 0.729-0.855) and 0.712 (95% CI: 0.603-0.822) in the training and test cohorts, respectively (Fig. 3A-3B). This model outperformed both PT model and the WL model (all Delong test $P < 0.05$ except for comparison with the WL model in the test cohort) (Fig. 4). The combined model, integrating the predicted probabilities derived from the clinical model and PTWL model (Supplementary Text 4), exhibited slightly higher predictive performance compared to the PTWL model, achieving AUCs of 0.810 (95% CI: 0.750–0.870) and 0.713 (95% CI: 0.600–0.827) in the training and test cohorts, respectively (Fig. 3A-3B). Nevertheless, no statistically significant difference in prediction efficiency was observed between the PTWL model and the combined model in the training and test cohorts (all $P > 0.05$) (Fig. 4). The combined model resulted in a sensitivity of 83.3%, specificity of 63.6%, positive predictive value (PPV) of 55.5%, negative predictive value (NPV) of 87.5%, and accuracy of 70.6% in the test cohort (Table 3).

The calibration curves for both the training and test cohorts demonstrated good consistency between the predicted and actual probabilities of the combined model, with $P > 0.05$ according to the Hosmer–Lemeshow tests (Fig. 3C-3D). The decision curve analysis was employed to evaluate the clinical utility of

models, and the results demonstrated that the combined model yielded higher net benefits across all evaluated models, indicating its superior efficacy in guiding therapeutic decisions (Fig. 3E-3F). Additionally, the superior performance of the combined model compared with other models was confirmed in the NRI test and IDI test (Table 4).

Subgroup analysis

To evaluate the robustness of the predictive model, a subgroup analysis was performed based on the treatment regimen across the entire cohort. The combined model maintained stable performance in both subgroups, and the Delong test indicated no statistically significant differences in its predictive efficacy between different treatment regimen subgroups (Figure S2, *P*=0.650), demonstrating consistent discriminative ability regardless of treatment type.

Survival analysis

Patients who did not experience positive events and had a minimum postoperative follow-up period of 1 year, along with all patients who experienced positive events, were included in the survival analysis. Among the 193 patients who satisfied this criterion, 33 patients (17.1%) died and 35 individuals (18.1%) exhibited disease recurrence during the observation period. The median follow-up time was 616 days (range of 29–2587days). Based on the optimal cutoff value (0.484) derived from maximizing Youden index of the combined model, we stratified the patients into high- and low-risk groups. The Kaplan-Meier survival curves revealed that low-risk group exhibited significantly longer RFS compared to high-risk group (*P* = 0.035), which was in line with the actual survival outcome (Fig. 5). The clinical utility of the combined model was demonstrated using two representative cases (Fig. 6).

Discussion

The pCR is regarded as a promising surrogate endpoint that may potentially serve as a substitute for long-term survival outcomes in patients with operable and resectable NSCLC following neoadjuvant immunotherapy. Notably, pCR demonstrates a robust correlation with 1- and 2-year event-free survival (EFS) [24]. Nevertheless, the clinical utility of biomarkers for accurately predicting pCR for neoadjuvant immunotherapy for NSCLC remains suboptimal, highlighting the imperative for more reliable predictive tools to optimize treatment decision-making and refine patient stratification in clinical practice. In this study, we developed and validated a whole lung radiomics model to predict pCR in NSCLC patients receiving neoadjuvant immunotherapy, which demonstrated predictive performance comparable to that of the tumor-specific radiomics model. In addition, the combined model incorporating whole lung radiomics features, tumor-specific radiomics features, and CEA levels showed enhanced predictive efficacy. These findings suggest that whole lung radiomics may serve as a valuable supplementary tool for identifying pCR in NSCLC patients undergoing neoadjuvant immunotherapy.

Previous studies have confirmed that baseline tumor radiomics features hold significant predictive value for assessing pCR in NSCLC patients receiving neoadjuvant immunotherapy [10, 11]. In this study, the PT

radiomics model exhibited promising predictive capability within the training cohort. However, when evaluated on the test cohort, its diagnostic accuracy declined to a mere 49.4%. A critical shortcoming identified was its low diagnostic specificity, which resulted in a high rate of false-positive findings—specifically, 70.9% of non-pCR patients were incorrectly identified as pCR responders. As a consequence, the overall predictive efficacy falls substantially below the standards required for reliable clinical application, and thus the model is unsuitable for supporting diagnostic or therapeutic decision-making in practice. Therefore, it is imperative to further explore multidimensional information to identify more robust and reliable biomarkers for the accurate prediction of treatment response.

The tumor microenvironment (TME) is a complex system comprising immune cells, stromal cells, the extracellular matrix, vasculature, lymphatic vessels, and signaling molecules, all of which play a critical role in the response to neoadjuvant immunotherapy. Studies have revealed that the tumor core is predominantly occupied by malignant cells, whereas the peripheral region is a hub for immune cells, cancer-associated fibroblasts, and other stromal components [25]. Given this spatial heterogeneity, research focus has expanded from the intratumoral region to the peritumoral compartment, with increasing evidence supporting the strong predictive value of peritumoral radiomics in patients with NSCLC receiving neoadjuvant immunotherapy [26]. Furthermore, a growing number of clinical studies have indicated that patients with LC-COPD often achieved a better prognosis from immunotherapy, likely due to an altered pulmonary immune microenvironment resulting from chronic inflammation [13, 16]. Although the technical feasibility of whole lung segmentation has been established [17], its value for predicting pCR to neoadjuvant immunotherapy in NSCLC remains unclear. In this study, we developed and validated a whole lung radiomics model for predicting pCR following neoadjuvant immunotherapy in NSCLC. Our results demonstrated that the whole lung radiomics model achieved superior predictive performance over the conventional tumor-specific model (AUC 0.671 vs. 0.593) with an excellent balance between sensitivity and specificity. To the best of our knowledge, this investigation represents the first report to establish the potential of whole lung radiomics as a non-invasive biomarker for predicting pCR to neoadjuvant immunotherapy in NSCLC patients.

A key innovation of this study lies in the development of a combined model integrating multimodal information—including whole lung radiomics, tumor-specific radiomics, and CEA levels—which achieved superior predictive performance compared to other models. This improvement was reflected in enhanced patient reclassification, as evidenced by improved patient reclassification (NRI) and enhanced discrimination between pCR and non-pCR patients (IDI). The combined model incorporated nine optimal radiomics features derived from the PTWL model, including six tumor-specific and three whole lung radiomics features. The tumor-specific radiomics features predict therapeutic response by quantifying intratumoral heterogeneity, where complex texture (e.g., ZoneEntropy) may suggest active immune cell infiltration, whereas disordered heterogeneity (e.g., RunVariance) indicates an immunosuppressive state [27]. The whole lung radiomics features provide complementary information by characterizing the pulmonary pathophysiological and immune state. For instance, a higher average density of the whole lung (e.g., WL_Wavelet-HHH_firstorder_Mean), resembling chronic inflammation, was associated with pCR. In contrast, extensive uniform low-density areas (e.g., WL_Wavelet-

LHH_GLSZM_LowGrayLevelZoneEmphasis), analogous to emphysema, correlated with poorer treatment response. Furthermore, higher variance indicating coexisting pathological changes (WL_log-sigma-1-mm-3D_GLDM_DependenceVariance), such as fibrosis and emphysema, was linked to an inferior response [17]. These three whole lung features carried substantial predictive weights, underscoring that the whole lung status is a critical determinant to predict therapeutic response of neoadjuvant immunotherapy in NSCLC. Based on the risk threshold established by the combined model, the follow-up cohort was stratified into high- and low-risk groups. Patients categorized into the low-risk group exhibited a significantly more favorable prognosis, characterized by a markedly reduced risk of recurrence and a significantly prolonged post-recurrence survival period. In contrast, individuals assigned to the high-risk group showed a substantially increased likelihood of recurrence and a correspondingly poorer prognosis over the follow-up period. Such prognostic disparities identified through risk stratification offer critical evidence-based medical support for the development of individualized treatment strategies.

There are several limitations in our study. Firstly, as a retrospective study, the potential for selection bias is inherent. Therefore, a prospective study is warranted. Furthermore, it is a single center study with a relatively limited sample size, multi-center validation should be performed to ensure the generalizability of the model. Finally, the biological rationale underlying the radiomics model, especially the whole lung radiomics model, necessitates further investigation in subsequent studies.

Conclusion

In conclusion, this study demonstrates that the whole lung radiomics is a promising biomarker for predicting pCR following neoadjuvant immunotherapy in NSCLC. The PTWL radiomics model, which integrates whole lung radiomics features with tumor-specific radiomics features, showed superior predictive performance for pCR, highlighting the complementary value of simultaneously assessing both local tumor characteristics and systemic host immunity condition. The combined model incorporating the predicted probabilities derived from the clinical model and PTWL radiomics model has the potential to guide personalized therapy decisions therapeutic decision-making for NSCLC patients, enabling pre-treatment risk stratification and identification of those who may benefit from neoadjuvant immunotherapy.

Abbreviations

NSCLC, non-small cell lung cancer

pCR, pathological complete response

PT, primary tumor

WL, whole lung

PTWL, primary tumor and whole lung

CEA, carcinoma embryonic antigen

RFS, recurrence-free survival

RECIST, response evaluation criteria in solid tumors

LN, lymph node

ROI, regions of interest

ICC, interclass correlation coefficient

ROC, receiver operating characteristic

AUC, area under curve

DCA, decision curve analysis

CI, confidence interval

OR, odds ratio

IQR, interquartile range

PPV, positive predictive value

NPV, negative predictive value

NRI, net reclassification improvements

IDI, integrated discrimination improvements

Declarations

Ethics approval and consent to participate

This retrospective study adhered to the Declaration of Helsinki. This retrospective study was approved by the Institutional Review Board of Tianjin Medical University Cancer Institute & Hospital (Approval No. bc20260290), and the requirement for written informed consent was waived.

Consent for publication

Not applicable.

Availability of data and materials

The relevant data of non-small cell lung cancer patients treated in our institution involved during the current research period can be obtained from the corresponding author upon reasonable request.

Competing interests

The authors have no relevant financial or non-financial interests to disclose.

Funding

This work was supported by the National Natural Science Foundation of China (Grant No. 82472063) and Tianjin Key Medical Discipline Construction Project（Grant No. TJYXZDXK-3-003A）

Author Contribution

Xiaoting Cai, Jingyi Yang, Qiliang Wang and Ying Liu conceived and designed the study. Xiaoting Cai and Jingyi Yang performed statistical analysis and interpretation. Xiaoting Cai drafted the manuscript. Fangyuan Qu, Jiahui E, Fan Liu and Yicai Zhang performed the data collection and cleaning. Bingsheng Sun and Ying Liu revised the article. All authors read and approved the final manuscript.

Acknowledgements

This work was supported by Follow-up Center of Tianjin Medical University Cancer Institute & Hospital.

References

1. Forde PM, Spicer JD, Provencio M, Mitsudomi T, Awad MM, Wang C, et al. Overall Survival with Neoadjuvant Nivolumab plus Chemotherapy in Lung Cancer. N Engl J Med. 2025;393:741–52. https://doi.org/10.1056/NEJMoa2502931
2. Cameron RB, Hines JB, Torri V, Porcu L, Donington J, Bestvina CM, et al. What is the ideal endpoint in early-stage immunotherapy neoadjuvant trials in lung cancer? Ther Adv Med Oncol. 2023;15:17588359231198446. https://doi.org/10.1177/17588359231198446
3. Forde PM, Spicer J, Lu S, Provencio M, Mitsudomi T, Awad MM, et al. Neoadjuvant Nivolumab plus Chemotherapy in Resectable Lung Cancer. N Engl J Med. 2022;386:1973–85. https://doi.org/10.1056/NEJMoa2202170
4. Provencio M, Nadal E, González-Larriba JL, Martínez-Martí A, Bernabé R, Bosch-Barrera J, et al. Perioperative Nivolumab and Chemotherapy in Stage III Non–Small-Cell Lung Cancer. N Engl J Med. 2023;389:504–13. https://doi.org/10.1056/NEJMoa2215530
5. Suijkerbuijk KPM, Van Eijs MJM, Van Wijk F, Eggermont AMM. Clinical and translational attributes of immune-related adverse events. Nat Cancer. 2024;5:557–71. https://doi.org/10.1038/s43018-024-00730-3
6. Lu F, Li X, Chen X, Liu Y, Liu H, Luo B, et al. MRI-based multiregional radiomics for pretreatment prediction of pathologic complete response to neoadjuvant chemoradiation therapy in locally

advanced rectal cancer: a bicenter study. Abdom Radiol [Internet]. 2025 [cited 2026 Feb 3]; https://doi.org/10.1007/s00261-025-05277-0

7. Zhou L, Zheng L, Zhang K, Guo X, Huang C, Zhu L, et al. Radiomic biomarkers for the recurrence prediction of hepatocellular carcinoma treated with postoperative TACE: A multicenter retrospective study. European Journal of Radiology. 2025;193:112442. https://doi.org/10.1016/j.ejrad.2025.112442
8. Bao X, Peng Q, Bian D, Ni J, Zhou S, Zhang P, et al. Short-term intra- and peri-tumoral spatiotemporal CT radiomics for predicting major pathological response to neoadjuvant chemoimmunotherapy in non-small cell lung cancer. Eur Radiol. 2025;35:6052–64. https://doi.org/10.1007/s00330-025-11563-8
9. Shi L, Li C, Bai Y, Cao Y, Zhao S, Chen X, et al. CT radiomics to predict pathologic complete response after neoadjuvant immunotherapy plus chemoradiotherapy in locally advanced esophageal squamous cell carcinoma. Eur Radiol. 2024;35:1594–604. https://doi.org/10.1007/s00330-024-11141-4
10. Liu C, Zhao W, Xie J, Lin H, Hu X, Li C, et al. Development and validation of a radiomics-based nomogram for predicting a major pathological response to neoadjuvant immunochemotherapy for patients with potentially resectable non-small cell lung cancer. Front Immunol. 2023;14:1115291. https://doi.org/10.3389/fimmu.2023.1115291
11. Yang M, Li X, Cai C, Liu C, Ma M, Qu W, et al. [18F]FDG PET-CT radiomics signature to predict pathological complete response to neoadjuvant chemoimmunotherapy in non-small cell lung cancer: a multicenter study. Eur Radiol. 2023;34:4352–63. https://doi.org/10.1007/s00330-023-10503-8
12. Mateu-Jimenez M, Curull V, Pijuan L, Sánchez-Font A, Rivera-Ramos H, Rodríguez-Fuster A, et al. Systemic and Tumor Th1 and Th2 Inflammatory Profile and Macrophages in Lung Cancer: Influence of Underlying Chronic Respiratory Disease. Journal of Thoracic Oncology. 2017;12:235–48. https://doi.org/10.1016/j.jtho.2016.09.137
13. Shin SH, Park HY, Im Y, Jung HA, Sun J, Ahn JS, et al. Improved treatment outcome of pembrolizumab in patients with nonsmall cell lung cancer and chronic obstructive pulmonary disease. Intl Journal of Cancer. 2019;145:2433–9. https://doi.org/10.1002/ijc.32235
14. Zhou J, Chao Y, Yao D, Ding N, Li J, Gao L, et al. Impact of chronic obstructive pulmonary disease on immune checkpoint inhibitor efficacy in advanced lung cancer and the potential prognostic factors. Transl Lung Cancer Res. 2021;10:2148–62. https://doi.org/10.21037/tlcr-21-214
15. Biton J, Ouakrim H, Dechartres A, Alifano M, Mansuet-Lupo A, Si H, et al. Impaired Tumor-Infiltrating T Cells in Patients with Chronic Obstructive Pulmonary Disease Impact Lung Cancer Response to PD-1 Blockade. Am J Respir Crit Care Med. 2018;198:928–40. https://doi.org/10.1164/rccm.201706-1110OC
16. Mark NM, Kargl J, Busch SE, Yang GHY, Metz HE, Zhang H, et al. Chronic Obstructive Pulmonary Disease Alters Immune Cell Composition and Immune Checkpoint Inhibitor Efficacy in Non–Small

Cell Lung Cancer. Am J Respir Crit Care Med. 2018;197:325–36. https://doi.org/10.1164/rccm.201704-0795OC

17. Zhou T-H, Zhou X-X, Ni J, Ma Y-Q, Xu F-Y, Fan B, et al. CT whole lung radiomic nomogram: a potential biomarker for lung function evaluation and identification of COPD. Military Med Res. 2024;11:14. https://doi.org/10.1186/s40779-024-00516-9
18. Yan M, Zhang Z, Tian J, Yu J, Dekker A, Ruysscher DD, et al. Whole lung radiomic features are associated with overall survival in patients with locally advanced non-small cell lung cancer treated with definitive radiotherapy. Radiat Oncol. 2025;20:9. https://doi.org/10.1186/s13014-025-02583-1
19. Rami-Porta R, Nishimura KK, Giroux DJ, Detterbeck F, Cardillo G, Edwards JG, et al. The International Association for the Study of Lung Cancer Lung Cancer Staging Project: Proposals for Revision of the TNM Stage Groups in the Forthcoming (Ninth) Edition of the TNM Classification for Lung Cancer. Journal of Thoracic Oncology. 2024;19:1007–27. https://doi.org/10.1016/j.jtho.2024.02.011
20. Leon-Ferre RA, Jonas SF, Salgado R, Loi S, De Jong V, Carter JM, et al. Tumor-Infiltrating Lymphocytes in Triple-Negative Breast Cancer. JAMA. 2024;331:1135. https://doi.org/10.1001/jama.2024.3056
21. Jiang H, Cannella R, Wu Z, Beaufrère A, Dioguardi Burgio M, Sartoris R, et al. Prognostic Implications of MRI-assessed Intratumoral Fat in Hepatocellular Carcinoma: An Asian and European Cohort Study. Radiology. 2024;313:e233471. https://doi.org/10.1148/radiol.233471
22. Mulkey F, Theoret MR, Keegan P, Pazdur R, Sridhara R. Comparison of iRECIST versus RECIST V.1.1 in patients treated with an anti-PD-1 or PD-L1 antibody: pooled FDA analysis. J Immunother Cancer. 2020;8:e000146. https://doi.org/10.1136/jitc-2019-000146
23. Gong X, Wang X, Wang L, Zeng X, Tang S, Cheng Y, et al. Comparing Multi– *b*- Value Diffusion MRI Models for Predicting Pathologic Complete Response to Neoadjuvant Chemotherapy in Breast Cancer. Radiology. 2025;316:e242969. https://doi.org/10.1148/radiol.242969
24. Hines JB, Cameron RB, Esposito A, Kim L, Porcu L, Nuccio A, et al. Evaluation of Major Pathologic Response and Pathologic Complete Response as Surrogate End Points for Survival in Randomized Controlled Trials of Neoadjuvant Immune Checkpoint Blockade in Resectable in NSCLC. Journal of Thoracic Oncology. 2024;19:1108–16. https://doi.org/10.1016/j.jtho.2024.03.010
25. Yan Y, Sun D, Hu J, Chen Y, Sun L, Yu H, et al. Multi-omic profiling highlights factors associated with resistance to immuno-chemotherapy in non-small-cell lung cancer. Nat Genet. 2025;57:126–39. https://doi.org/10.1038/s41588-024-01998-y
26. Lin X, Liu Z, Zhou K, Li Y, Huang G, Zhang H, et al. Intratumoral and peritumoral PET/CT-based radiomics for non-invasively and dynamically predicting immunotherapy response in NSCLC. Br J Cancer. 2025;132:558–68. https://doi.org/10.1038/s41416-025-02948-z
27. Liu L, Gao F, Li Y, Cheng J, Zhang H, Cai P, et al. An Interpretable Radiomics-Based Model Using Susceptibility-Weighted Imaging for Non-Invasive Prediction of Tertiary Lymphoid Structures in Hepatocellular Carcinoma. JHC. 2025;Volume 12:2197–211. https://doi.org/10.2147/JHC.S551462

Tables

Tables 1 to 4 are available in the Supplementary Files section.

Figures

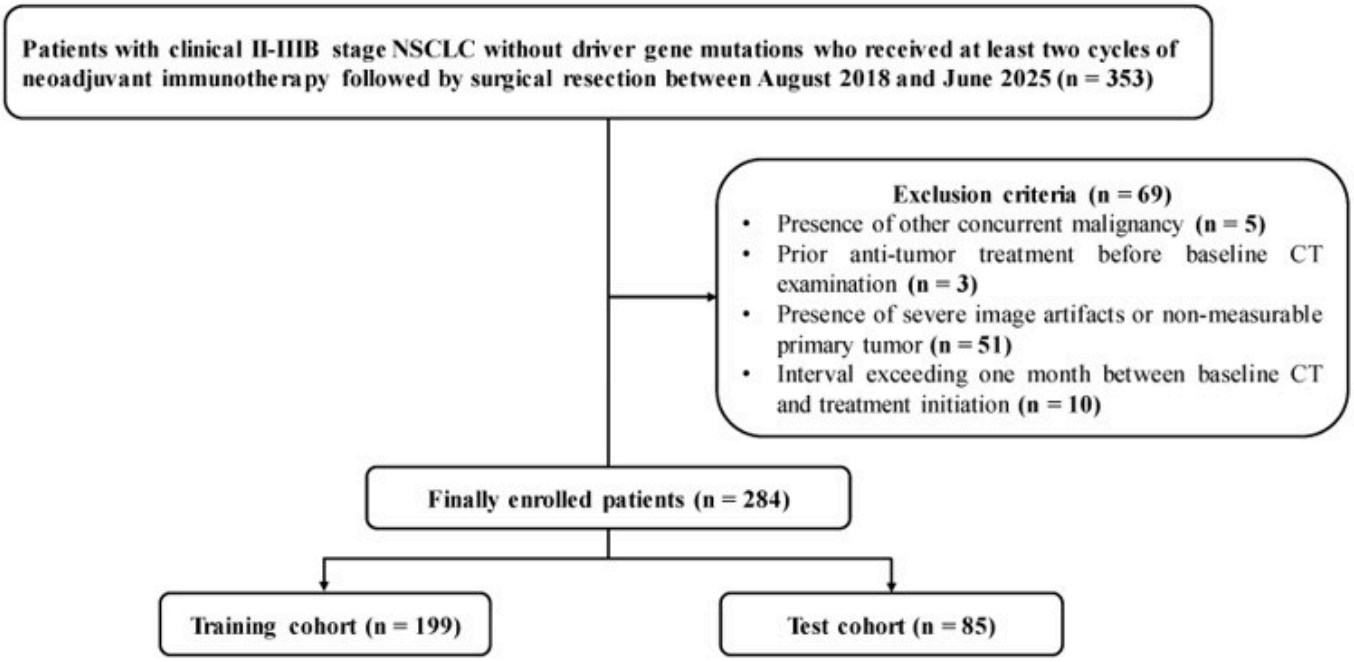


Figure 1

Flowchart of patient eligibility and exclusion criteria.

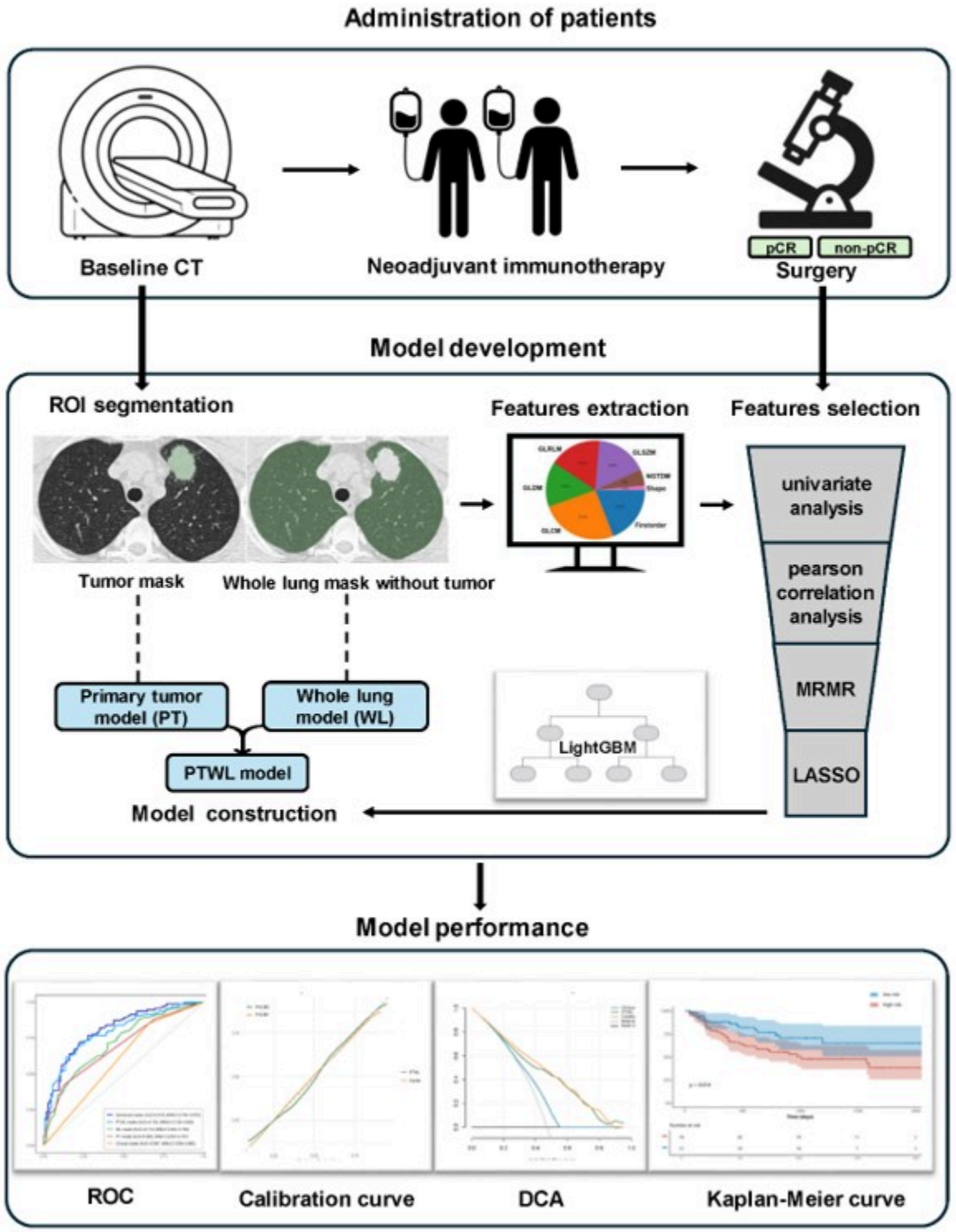


Figure 2

Illustration of the study design. pCR = pathological complete response, ROI = region of interest, MRMR = Minimum Redundancy Maximum Relevance, LASSO = Least Absolute Shrinkage and Selection Operator, ROC = receiver operating characteristic curve, DCA = Decision curve analysis.

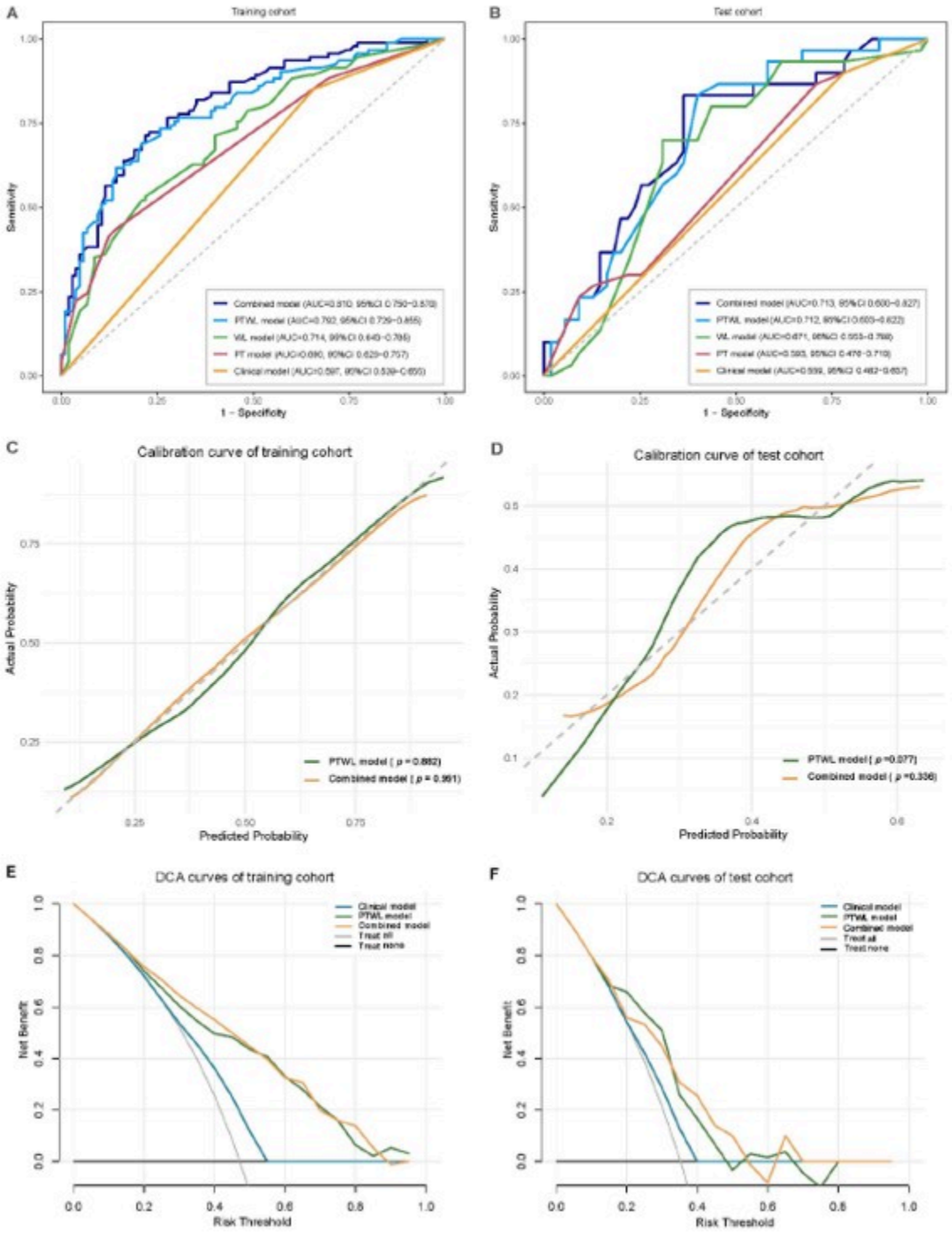


Figure 3

Predictive performance and clinical usefulness of different models for predicting pCR in the training and test cohorts. The ROC curves of different predictive models in the training cohort **(A)** and the test cohort **(B)**. The calibration curves of different predictive models in the training cohort **(C)** and the test cohort **(D)**. The decision curves of different predictive models in the training cohort **(E)** and the test cohort **(F)**.

PT = primary tumor radiomics model, WL = whole lung radiomics model, PTWL = primary tumor plus whole lung radiomics model.

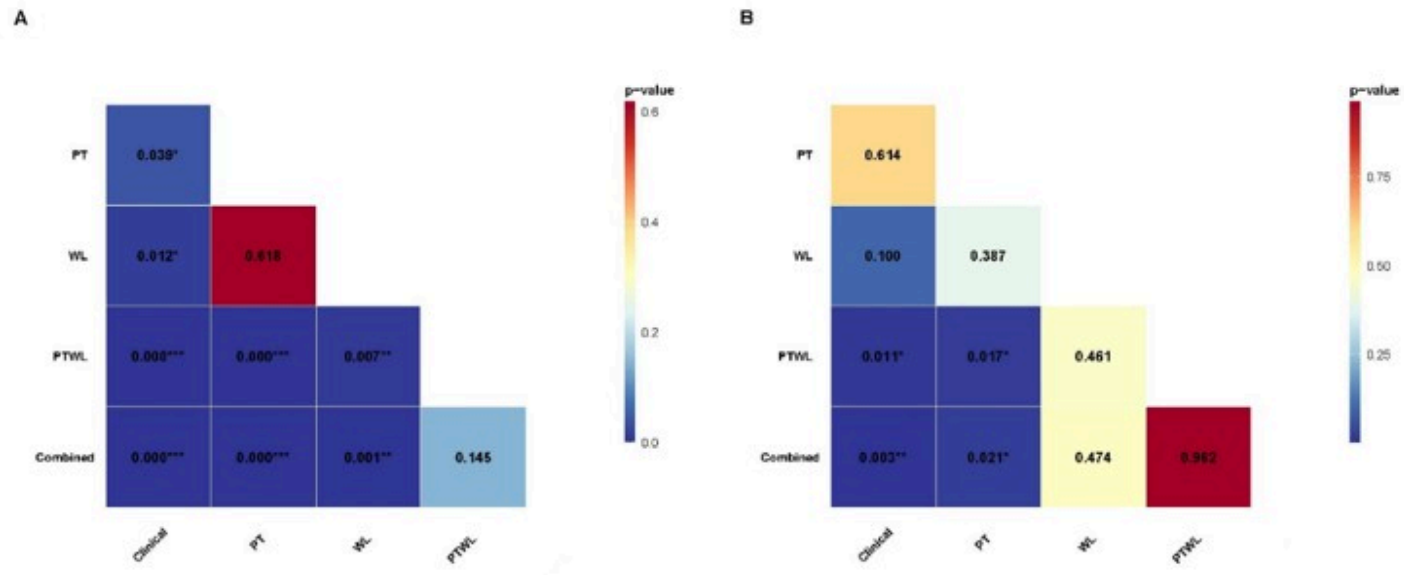


Figure 4

Delong test between different models in the training cohort **(A)** and the test cohort **(B)**. PT = primary tumor radiomics model, WL = whole lung radiomics model, PTWL = primary tumor plus whole lung radiomics model.

* *P*-value≤0.05; ** *P*-value≤0.01; *** *P*-value≤0.001

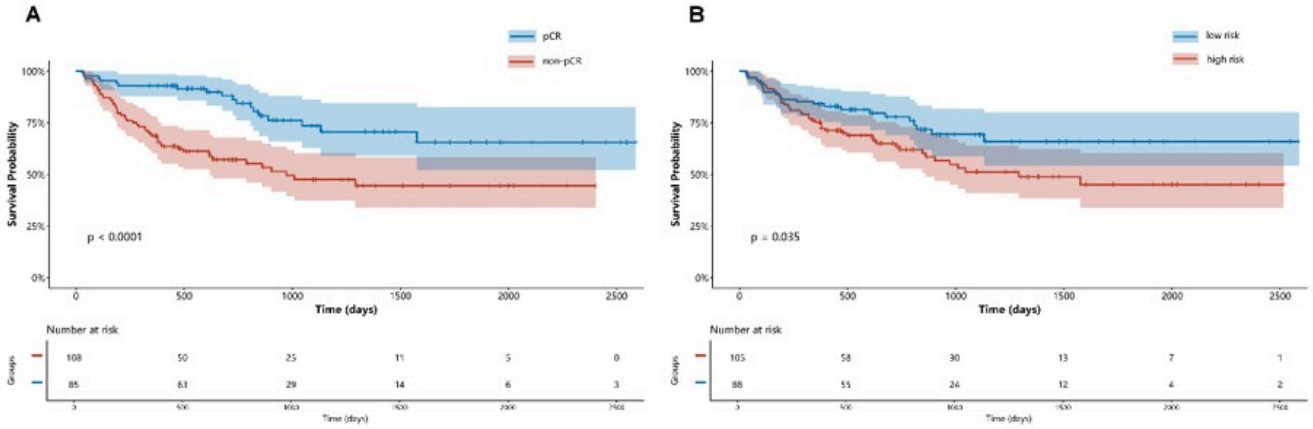


Figure 5

Kaplan–Meier curves for the recurrence-free survival (RFS) between pCR vs non-pCR groups **(A)** and combined model predicted high risk vs low-risk groups **(B)**.

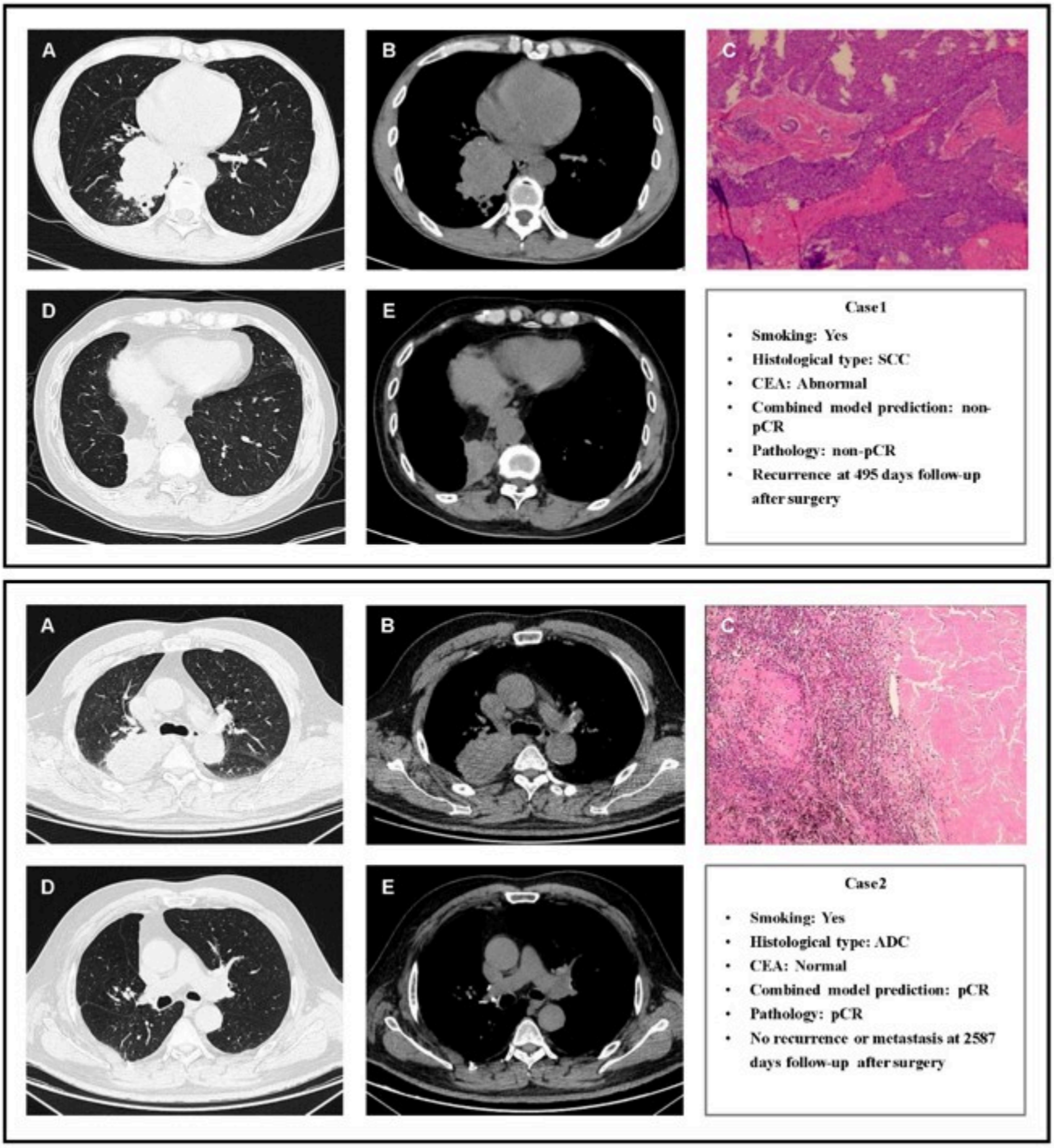


Figure 6

Individual applications of the combined model to predict therapeutic response. In case 1, a patient underwent a pre-treatment CT examination **(A-B)**. The combined model predicted a non-pCR outcome, which was subsequently confirmed by postoperative pathology **(C)**, with the tumor recurrence occurring at 495 days after surgery**(D-E)**. In case 2, a patient underwent a pre-treatment CT examination **(A-B)**. The

combined model predicted a pCR outcome, which was subsequently confirmed by postoperative pathology **(C)**, with no recurrence or metastasis at 2587 days after surgery **(D-E)**.

Supplementary Files

This is a list of supplementary files associated with this preprint. Click to download.

- supplementarymaterials.docx
- Tables.docx